AIAA JOURNAL
Vol. 35, No. 5, May 1997

Behavior of Wake Vortices Near Ground

Alexandre Corjon*
Centre Européen de Recherche et Formation Avancée en Calcul Scientifique, Toulouse Cedex F-31057, France
and
Thierry Poinsot†
Institut de Mécanique des Fluides de Toulouse, Toulouse Cedex F-31400, France

Direct numerical simulations of a vortex pair embedded in a stable atmospheric boundary layer are presented. The effects of various crosswind conditions are studied. These computations demonstrate the creation of secondary vortices for the range of Reynolds number ($3.77 \times 10^3 \leq Re_\Gamma \leq 1.131 \times 10^5$). The physics of wake vortex interactions with the ground for different values of crosswind are discussed. The redistribution of vorticity between the atmospheric boundary layer and the vorticity induced by the primary vortices may explain the vortex tilting phenomenon. A parameterization of the effect of crosswind on the minimum altitude reached by the two vortices is given.

Nomenclature

b	= wingspan
b_0	= initial spacing between primary vortices, $\pi/4b$ for an elliptically loaded wing
c	= speed of sound, $\sqrt{(\gamma RT)}$
d_0	= reference spacing between primary vortices
g	= stream-function coefficient of Lamb vortex
h	= altitude of vortices
$h_{\min}$, $h^0_{\min}$	= minimum altitude of vortices
nx, ny	= number of grid points in x and y directions
R	= constant
Re_v	= Reynolds number
Re_Γ	= circulation-based Reynolds number, Γ/ν
r_c	= core radius
T	= temperature
t	= time
U	= velocity of crosswind
$U^*_{\max}$	= normalized maximal velocity of crosswind
U_0	= crosswind magnitude at initial height
u_f	= friction velocity
$u_{\theta\max}$	= maximal tangential velocity of the vortex
W_S, w_s	= dimensionless parameters
x, y, z	= ground coordinates
y_r	= roughness height
Γ	= circulation of individual vortex
γ	= ratio of specific heat
κ	= von Kármán constant (=0.4)
ν	= kinematic viscosity
σ	= wind shear

Subscripts

c	= core
0	= initial

Superscript

$*$	= normalized number

Introduction

WITH increased traffic growth and the design of new high-capacity aircraft, problems related to wake vortices are becoming more and more important. Throughout the world, new studies on those problems are being initiated. Regulatory authorities are interested in developing air traffic systems that enable the reduction of the spacing between aircraft during landing and take-off so as to increase airport capacity. Aircraft manufacturers have a vested interest in alleviating wake vortices to avoid categorization problems that could lead to the less efficient use of high-capacity aircraft. For this reason, they need to understand wake vortex behavior near the ground for given meteorological conditions. This knowledge has to be implemented in an engineering model to permit real-time evaluation of hazards associated with wake vortices (position and strength). There are numerous external effects that contribute to wake vortex evolution and hence many literature references to the subject. In 1970, Crow[1] studied the stability of a vortex pair, and his results relate the vortex linking time to the turbulent dissipation rate. These results were confirmed experimentally.[2–4] In 1975, Donaldson and Bilanin[5] provided a comprehensive study of wake vortices and phenomena enhancing their decay: atmospheric turbulence, stratification, and vertical wind shear. They proposed a simple formula to relate the vortex decay and the atmospheric turbulence, which is commonly used in engineering models.[6] The works of Hill,[7] Sarpkaya,[8] and, more recently, Spalart[9] deal with stratification effects.

None of those studies consider ground effects, even if the hazard is more severe near the ground because of the short recovery time available. It has been shown that the greatest frequency of reported incidents concerns following aircraft in the 100–200-ft altitude range, where trailing vortices are submitted to ground effect.[10] This can be explained by the fact that all aircraft follow the same flight path, whereas vortices may bounce on the ground; the behavior of the wake vortices then depends strongly on the velocity of the crosswind. The work reported here is focused on the viscous ground effect on the trailing vortex trajectories with crosswind. Some numerical studies already have been published on wake vortex rebound but none tries to quantify the relationship between crosswind and rebound.[11–14] Some authors provide two-dimensional turbulence simulations[11,15,16] but are unable to describe correctly complex three-dimensional phenomena.[17,18]

The interactions between a vortex and a wall are of interest for many applications.[19] This study considers its application to an engineering model called VORTEX[20] and permits us to define the minimum altitude reached by the vortices for the problem of wake vortex hazards. A first version of VORTEX was based on Greene's model[6] for stratification and atmospheric turbulence effects and included the effects of the ground and crosswind. This model assumes that the vortex sheet shed by the aircraft has completely rolled up and that only two counter-rotating vortices remain in the atmosphere. As in the model first presented by Tombach,[4] the vorticity is assumed to be concentrated into two counter-rotating vortex cores whose diameters

Received Jan. 18, 1996; revision received Jan. 15, 1997; accepted for publication Jan. 30, 1997.

*Senior Researcher, 42, av. G. Coriolis. E-mail: corjon@cerfacs.fr. Member AIAA.

†Computational Fluid Dynamics Team Manager. E-mail: poinsot@cerfacs.fr. Member AIAA.

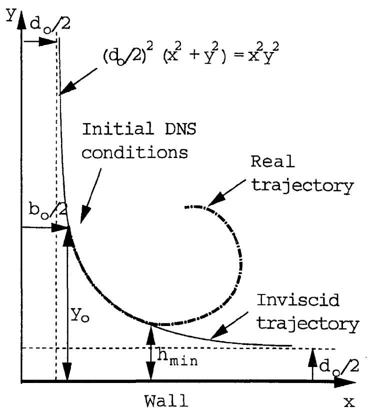

Fig. 1 Comparison between inviscid and real trajectory.

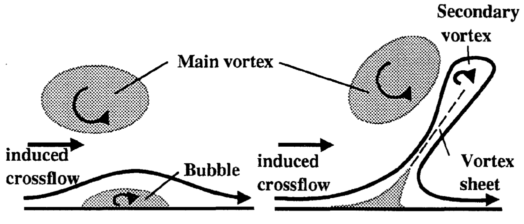

Fig. 2 Viscous ground effect.

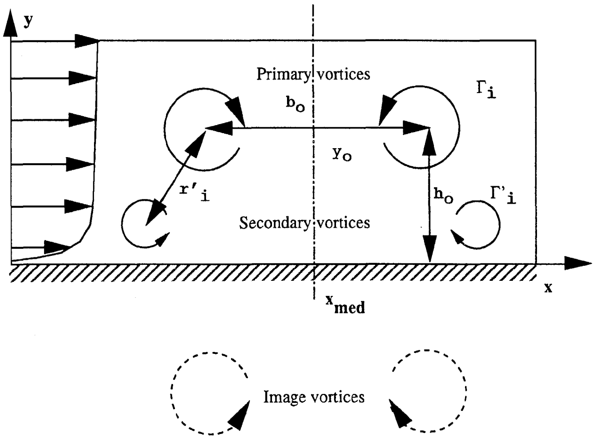

Fig. 3 Computation domain.

are small compared to their spacing, so that they can be modeled as point vortices. The transport of the trailing vortices is modeled by the laminar potential flow solution of infinite line vortices. This solution indicates that, without ground effect, the two vortices will descend while maintaining a constant distance d_0 (see Fig. 1).

The first effect of the ground is to make the pair diverge and is due to an inviscid phenomenon: the effect of the ground plane can be modeled by two image vortices whose strengths are equal and opposite to those of the real vortices to satisfy the slip boundary condition on the wall in the inviscid theory. When the real vortex and its image are close enough, their mutual interaction has a greater importance than the interaction of the two real vortices.

The second effect of the ground is a viscous effect. Experiments[21,22] show that the trajectory of the vortices near the ground in the atmosphere differs from the inviscid trajectory. Barker and Crow[23] asserted that the rebound was due to the finite vortex core size, but Saffman[24] has shown that the bouncing of the vortices could not be explained in the framework of inviscid theory. The explanation proposed by Harvey and Perry[22] (which was confirmed by many theoretical studies of a vortex pair under ground effect[2,25,26]) is based on viscous phenomena at the wall and is described in Fig. 2.

During their descent, each primary vortex induces a boundary layer. As they continue to descend, this vorticity sheet detaches from the wall, creating a secondary vortex. This secondary vortex rolls over the primary one and makes it rise.

In VORTEX,[20] classic two-dimensional inviscid theory is modified (as proposed by Liu[2]) to introduce vortex rebound. A line vortex is added near the wall to model the effect of the secondary vortex. This method introduces three new parameters (see notations in Fig. 3) in VORTEX:

1) $r'_i = b_0/2$: the distance between the primary vortex i and its secondary vortex; b_0 is the initial spacing between the two primary vortices; r'_i is supposed to be constant.[2,20]

2) Γ'_i: circulation of the secondary vortex.

3) h_0: altitude of rebound.

The altitude of rebound h_0 is the altitude that must be reached by the primary vortex to introduce the secondary vortex near the ground. It is usually estimated by $h_0 = 0.6b_0$ (Ref. 2).

If the two first parameters are well defined, the third (the altitude h_0) depends on the value of the crosswind.[20] The following work presents two-dimensional, direct numerical simulations of vortex rebound with or without crosswind. The physics of vortex rebound and the influence of crosswind on the minimum altitude reached by the wake vortices are described, and a tentative parameterization of the altitude of rebound h_0 as a function of crosswind shear is proposed.

Methodology

For the direct numerical simulations (DNS), we use the NTMIX[27] Navier–Stokes solver. The aims of these computations are to understand vortex rebound mechanisms and to derive a simple model for rebound to be used in engineering codes. Our aim is to study the rebound of wake vortices embedded within a stable atmospheric boundary layer. This configuration is representative of meteorological conditions in the morning when the sun has not yet heated up the ground. In this case, the atmospheric boundary layer is rather small ($\leq$100 m) and is not highly turbulent. Then the assumption of laminar interaction is valid. The three-dimensional effects will have to be estimated at a later stage[18] with the effects of turbulence for a convective atmospheric boundary layer. We concentrate on the altitude of rebound, and the results presented by Zheng and Ash[16] show that the altitude of rebound is the same for laminar and turbulent cases without crosswind at a circulation-based Reynolds number $Re_\Gamma = \Gamma/\nu = 7.5 \times 10^3$ or 7.5×10^4.

NTMIX solves the fully compressible two-dimensional Navier–Stokes equations. High-order compact schemes of spectral-like resolution are used for the spatial differencing and a third-order Runge–Kutta method is used for time integration.[28,29] The numerical scheme (sixth order in space and third order in time) is used in conjunction with the NSCBC (Navier–Stokes characteristic boundary conditions) method to define the boundary conditions[29] and is very accurate. More details on test-case computations can be found in Poinsot and Lele.[29] To test the accuracy of our results, we have undertaken a grid independence study reported in the section "Expression of Rebound Height."

Lamb's vortices are used for the initialization. The associated stream function is

$$\psi = -g \ln(r^2 + r_c^2)$$

where g is related to the vortex circulation $\Gamma = 4\pi g$. The Reynolds number of each vortex is

$$Re = \frac{u_{\theta\max} r_c}{\nu} = \frac{g}{\nu} = \frac{\Gamma}{4\pi\nu}$$

The initialization involves four vortices (see Fig. 3): two real vortices and their mirror images to ensure a zero normal velocity at the wall. The no-slip condition is imposed by setting a zero tangential velocity at the wall. This setting is made by multiplying the velocity induced by the vortices with a function

$$\sin\left(\frac{\pi y}{2y_{\text{ref}}}\right)^{\frac{1}{6}} \qquad \text{for} \qquad y \in [0, y_{\text{ref}}]$$

The boundary conditions are as follows:

1) inlet—subsonic inlet or nonreflecting

$$u = U(y) = \frac{u_f}{\kappa}\log\left(\frac{y + y_r}{y_r}\right)$$

Table 1 Parameters of test cases

Case	b_0/b	g/cb	r_c/b	$U(y_{\max})/c$	x_{med}/b	y_0/b	d_0/b	Re_{ref}	$u_{\theta_{\max}}$	Re_v	nx	ny
1	0.8	0.03	0.1	0.00	0.0	1.0	0.74	2×10^4	0.3	6×10^2	257	121
2	0.8	0.03	0.1	0.05	2.0	1.0	0.74	2×10^4	0.3	6×10^2	363	121
3	0.8	0.03	0.1	0.10	1.4	1.0	0.74	2×10^4	0.3	6×10^2	363	121
4	0.8	0.03	0.1	0.20	1.4	1.0	0.74	2×10^4	0.3	6×10^2	363	121
5	0.6	0.03	0.1	0.10	1.4	1.0	0.57	2×10^4	0.3	6×10^2	363	121
6	0.6	0.03	0.1	0.20	1.4	1.0	0.57	2×10^4	0.3	6×10^2	363	121
7	0.8	0.02	0.1	0.05	1.4	1.0	0.74	2×10^4	0.2	4×10^2	363	121
8	0.8	0.02	0.1	0.10	1.4	1.0	0.74	2×10^4	0.2	4×10^2	363	121
9	0.8	0.015	0.1	0.05	1.4	1.0	0.74	2×10^4	0.15	3×10^2	363	121
10	0.8	0.045	0.15	0.00	3.0	1.0	0.74	2×10^4	0.3	9×10^2	363	121
11	0.6	0.045	0.15	0.00	3.0	1.0	0.57	2×10^4	0.3	9×10^2	363	121
12	0.8	0.03	0.15	0.00	3.0	1.0	0.74	2×10^4	0.2	6×10^2	363	121
13	0.6	0.03	0.10	0.00	3.0	1.0	0.57	2×10^4	0.3	6×10^2	363	121

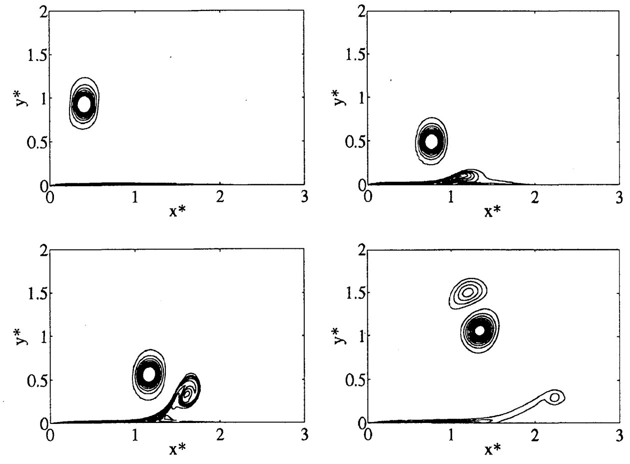

Fig. 4 Contours of vorticity: $U^* = 0.00$ (case 1) at $t'' = 0.00, 5.38, 8.03$, and 15.05; $\Delta\omega^* = 0.5$; $\omega^* \in [-5, 5]$.

or

$$u = U(y) = \frac{U(y_{\max})}{\log(y_{\max}/y_r)} \log\left(\frac{y + y_r}{y_r}\right)$$

2) outlet—nonreflecting (convective and acoustic waves exit with negligible reflection)
3) bottom—nonslip wall
4) top—nonreflecting

The inlet wind profile is given by Monin–Obukhov similarity theory for the surface boundary layer.[30] It corresponds to neutral condition in the surface boundary layer ($y \le 100$ m).

All lengths are normalized using the wingspan b. The initial spacing b_0 is set to $0.8b$, which is the same as for a wing with an elliptical loading[31] [$b_0 = (\pi/4)b$]. The domain size for all computations is ($0 < x^* < 6$, $0 < y^* < 2$).

The results are presented using a dimensionless time t'' equal to $u_{\theta_{\max}} t/b_0$. Velocities are scaled using the speed c, and the computation Reynolds number is $Re_{\text{ref}} = cb/\nu$.

Results

Contours of Vorticity

Table 1 presents the parameters of the 13 test cases used to study the effects of crosswind on the rebound of a vortex pair. The circulation-based Reynolds number varies between 3.77×10^3 and 1.131×10^4. The spatial discretization is in the x direction ($\Delta x = 0.111 r_c$ or $0.167 r_c$) and in the y direction ($\Delta y = 0.111 r_c$ or $0.167 r_c$ or $0.083 r_c$).

Figure 4 presents the results obtained without crosswind [$U^*_{\max} = U(y_{\max})/c = 0.00$] at four different times: $t'' = 0.00, 5.38, 8.03$, and 15.05 (see Table 1, case 1).

The initial conditions are $g^* = g/(bc) = 0.03$, $r^*_c = r_c/b = 0.1$ (core radius), $b^*_0 = b_0/b = 0.8$, and $x^*_{\text{med}} = 0$.

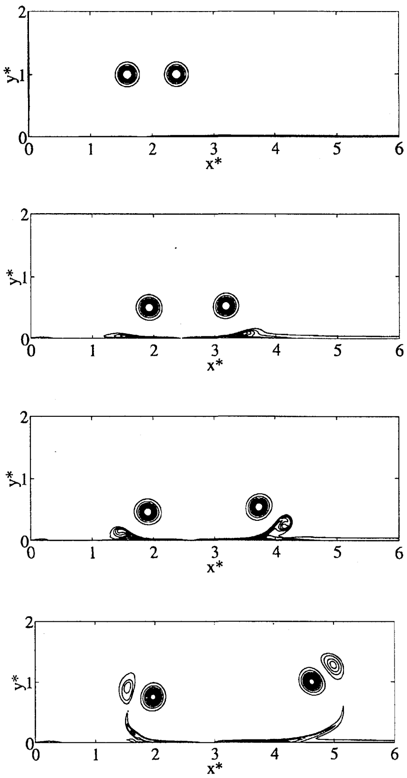

Fig. 5 Contours of vorticity: $U^*_{\max} = 0.05$ (case 2) at $t'' = 0.00, 4.50, 6.75$, and 11.25; $\Delta\omega^* = 0.5$; $\omega^* \in [-5, 5]$.

The vortex Reynolds number $Re_v = r_c u_{\theta_{\max}}/\nu$ is equal to 6×10^2. The contours of vorticity $\omega^* = \omega b/c$ are drawn from -5 to 5 with a step $\Delta\omega^* = 0.5$.

The rebound mechanism is in agreement with the explanation of Harvey and Perry.[22] The vortex creates a wall boundary layer with a strong vorticity sheet while descending. The separated vorticity sheet is elongated until it breaks and creates a secondary vortex. This vortex rolls over the primary one and makes it rise. These results are in good agreement with Orlandi's work[26] (note that the Reynolds numbers of the two computations are slightly different: $Re_v = 6 \times 10^2$ here and $Re_v = 8 \times 10^2$ for Orlandi).

Figures 5–7 present the results obtained for three values of crosswind: $U^*_{\max} = 0.05$, i.e., $u^*_{\theta_{\max}}/U^*_{\max} = 6$ (case 2); 0.10, i.e., $u^*_{\theta_{\max}}/U^*_{\max} = 3$ (case 3); and 0.20, i.e., $u^*_{\theta_{\max}}/U^*_{\max} = 1.5$ (case 4). The initial conditions of the computations are the same for the vortices: $g^* = 0.03$, $r^*_c = 0.1$, and $b^*_0 = 0.8$. The maximal values of the logarithmic profile of crosswind are different (see the preceding), as well as the value of x^*_{med} ($x^*_{\text{med}} = 2$ for $U^*_{\max} = 0.05$, and $x^*_{\text{med}} = 1.4$ for the two other values).

Figure 5 (case 2) presents the evolution of vorticity at four instants: $t'' = 0.00, 4.50, 6.75$, and 11.25. The observed mechanism is

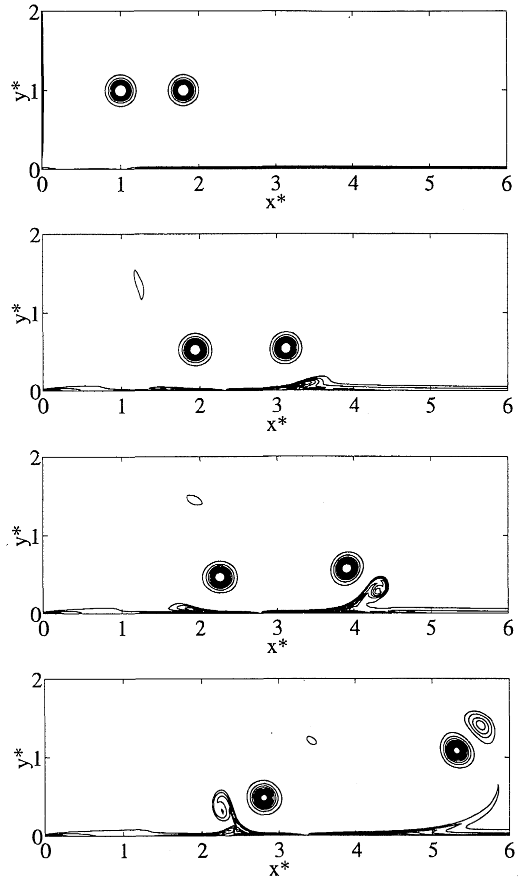

Fig. 6 Contours of vorticity: U^*_{max} = 0.10 (case 3) (see caption of Fig. 5).

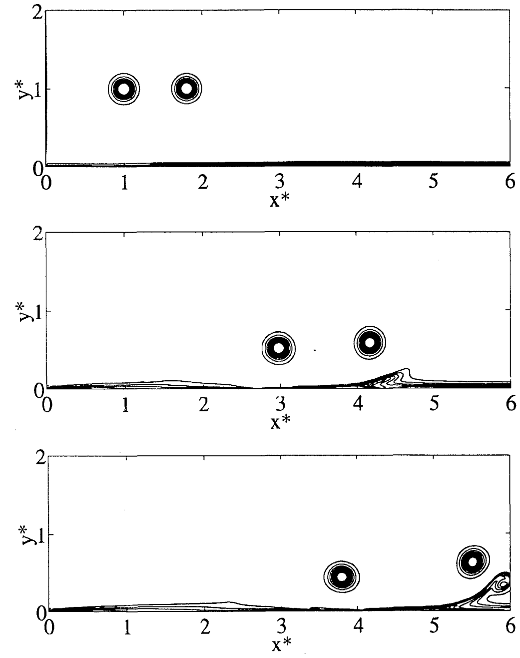

Fig. 7 Contours of vorticity: U^*_{max} = 0.20 (case 4) (see caption of Fig. 5).

the same as in Fig. 4. Because of their mutual interaction, the two primary vortices descend and create a strong vorticity sheet. As the vortices move down, because of the adverse pressure gradient, the boundary layers separate and create the secondary vortices.

The main difference with the case without crosswind is the asymmetry for the upwind (left) and downwind (right) vortex pair. The vorticity of the downwind secondary vortex has the same sign as the vorticity due to the crosswind, and separation is favored. On the

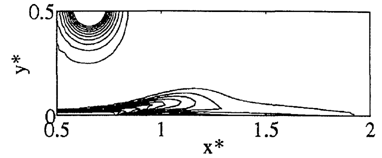

a) U^*_{max} = 0 (case 1)

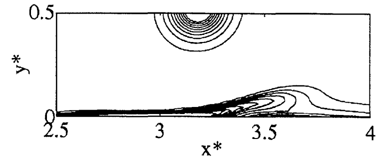

b) U^*_{max} = 0.05 (case 2)

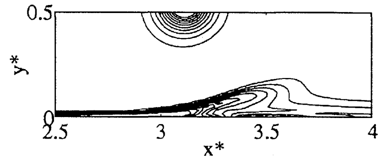

c) U^*_{max} = 0.10 (case 3)

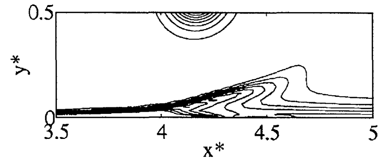

d) U^*_{max} = 0.20 (case 4)

Fig. 8 Zoom of contours of vorticity for the downwind vortex at t'' = 4.5; $\Delta\omega^*$ = 0.5; $\omega^* \in [-5, 5]$.

contrary, the separation is delayed for the upwind secondary vortex with the opposite sign of the vorticity due to the crosswind.

Figure 6 (case 3) shows the contours of vorticity in the case of a crosswind equal to $U^*_{max} = 0.10$. In this case the velocity of the crosswind is one-third of the maximal tangential velocity $u_{\theta_{max}}$ of the vortices (see Table 1). The behavior of the vortices described above is then more obvious. The asymmetry between the upwind and downwind secondary vortices is stronger, and at $t'' = 11.25$, as the downwind pair moves away from the wall, the secondary vortex for the upwind pair has not yet detached. At this time, a tertiary vortex with the same sign of vorticity as the primary also is observed near the upwind vortex.

Finally, Fig. 7 (case 4) shows the evolution for a crosswind of $U^*_{max} = 0.20$. For this case, the crosswind is high (two-thirds of the maximal tangential velocity of the vortices). At $t'' = 6.75$, the secondary vortex for the upwind vortex is not created. The opposite vorticity of that due to the crosswind is able to counteract the effect of the descending upwind primary vortex.

The effect of crosswind on the boundary layers induced by the primary vortices may be observed during the separation for the downwind vortex (Fig. 8) and the upwind one (Fig. 9): All snapshots are made at the same time $t'' = 4.5$ and illustrate differences in the evolution of the vorticity near the ground plane. For the downwind pair (Fig. 8), the trace of the tertiary vortex can be seen, just below the secondary vortex. This trace is less obvious as the crosswind speed increases. When the crosswind velocity increases, separation occurs earlier. For $U^*_{max} = 0.20$ (Fig. 8d), the vorticity sheet is more elongated and the primary vortex is at a higher altitude than in the other cases.

The vorticity induced by the crosswind, which is important near the ground plane, counteracts the creation of the secondary vortex. For a crosswind of $U^*_{max} = 0.20$ (Fig. 9d), the rebound of the upwind vortex will certainly never occur.

This kind of behavior is observed by Luton et al.[14] They studied the interaction of spanwise vortices with a boundary layer. Their initial conditions are totally different but the physics of the observed phenomenon is quite similar. They considered the interaction

Table 2 Parameters of test cases without crosswind

Case	b_0/b	g/cb	r_c/b	$x_{\rm med}/b$	y_0/b	d_0/b	$Re_{\rm ref}$	$u_{\theta_{\max}}$	Re_v	nx	ny
01	0.8	0.015	0.10	3.0	1.0	0.74	2×10^4	0.15	3×10^2	363	121
02	0.8	0.015	0.15	3.0	1.0	0.74	2×10^4	0.1	3×10^2	363	121
03	0.6	0.015	0.10	3.0	1.0	0.57	2×10^4	0.15	3×10^2	363	121
04	0.6	0.015	0.15	3.0	1.0	0.57	2×10^4	0.1	3×10^2	363	121
05	0.8	0.020	0.10	3.0	1.0	0.74	2×10^4	0.2	4×10^2	363	121
06	0.8	0.020	0.15	3.0	1.0	0.74	2×10^4	0.133	4×10^2	363	121
07	0.6	0.020	0.10	3.0	1.0	0.57	2×10^4	0.2	4×10^2	363	121
072	0.6	0.020	0.10	3.0	1.0	0.57	2×10^4	0.2	4×10^2	363	241
08	0.6	0.020	0.15	3.0	1.0	0.57	2×10^4	0.133	4×10^2	363	121
09	0.8	0.030	0.10	3.0	1.0	0.74	2×10^4	0.3	6×10^2	363	121
10	0.8	0.030	0.15	3.0	1.0	0.74	2×10^4	0.2	6×10^2	363	121
11	0.6	0.030	0.10	3.0	1.0	0.57	2×10^4	0.3	6×10^2	363	121
12	0.6	0.030	0.15	3.0	1.0	0.57	2×10^4	0.2	6×10^2	363	121
13	0.8	0.045	0.10	3.0	1.0	0.74	2×10^4	0.45	9×10^2	363	121
14	0.8	0.045	0.15	3.0	1.0	0.74	2×10^4	0.3	9×10^2	363	121
15	0.6	0.045	0.10	3.0	1.0	0.57	2×10^4	0.45	9×10^2	363	121
152	0.6	0.045	0.10	3.0	1.0	0.57	2×10^4	0.45	9×10^2	363	241
16	0.6	0.045	0.15	3.0	1.0	0.57	2×10^4	0.3	9×10^2	363	121

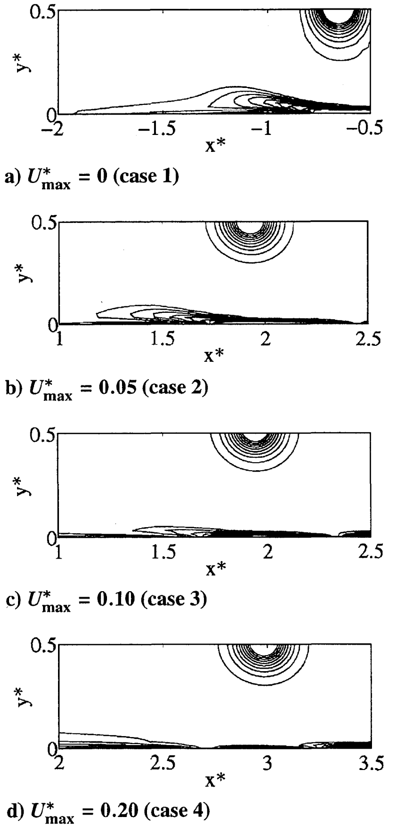

Fig. 9 Zoom of contours of vorticity for the upwind vortex at $t'' = 4.5$; $\Delta\omega^* = 0.5$; $\omega^* \in [-5, 5]$.

between only one vortex with positive or negative vorticity at lower Reynolds number ($Re_\Gamma = 1.097 \times 10^2$ or 3.952×10^2) and a boundary layer with higher velocity ($u^*_{\theta_{\max}}/U^*_{\max} = 0.5$ or 1.8). Furthermore, the vortex is not embedded in the boundary layer.

Three cases are presented, two corresponding to an upwind vortex and one corresponding to a downwind vortex.[14] They show that the high level of vorticity of the boundary layer can counteract the eruption of fluid. For the downwind configuration, there is an eruption but no secondary vortex (probably because of the small Reynolds number of the computation $Re_\Gamma = 1.097 \times 10^2$).

Our computations confirm their conclusions for higher Reynolds number and lower velocity of the boundary layer. Here the main movement of the primary vortices is controlled by the initial spacing of the vortex pair and the minimum altitude is always higher than in their computations.

Rebound Height in Absence of Crosswind

An important aspect of simple models for vortex evolution is to parameterize the altitude of rebound (Fig. 1).

Definition of Reference Spacing d_0

Far from the wall, the vortex pair propagates with a constant vortex spacing d_0 (which we call the reference spacing) which is the relevant parameter for initial conditions. However, because of resolution requirements, the vortex pair is sometimes initialized at an altitude y_0 and a vortex spacing b_0 such that the influence of the wall is already felt.

The reference spacing d_0 may be deduced from y_0 and b_0 using the vortex trajectory in the inviscid theory[32]:

$$(d_0/2)^2(x^2 + y^2) = x^2y^2$$

so that the reference vortex spacing d_0 is given by

$$d_0 = \frac{2b_0y_0}{\sqrt{b_0^2 + 4y_0^2}}$$

We use this length d_0 to normalize the altitude of rebound.

Expression of Rebound Height

Table 2 presents the parameters of the test cases used to express the rebound height $h^0_{\min}$ in the absence of crosswind.

The altitude h_0 is searched as a function of Re_v and r_c/d_0 vs the Reynolds number Re_v. The nondimensional value of h_0 is presented in Fig. 10 for four values of r_c/d_0. The error due to the determination of the minimum altitude reached in the computation could explain the difference in the results. There is only a difference of one grid point between the results for a given d_0. The value of $0.65d_0$ for $h^0_{\min}/d_0$ seems to be a good estimator of the viscous effect on the rebound. The value found by Zheng and Ash[16] is about $0.67d_0$. Peace and Riley[33] found higher values, but only two Reynolds number were tested: $Re_\Gamma = 0.5 \times 10^2$ and 10^2. They also indicate that within the range of values of Re_v considered, flow separation from the wall does not take place.

Here we clearly see the flow separation, and it seems that the minimum altitude will be lower as the Reynolds number Re_v increases.

Grid independency was checked by doubling the number of grid points in the y direction for cases 7 and 15 (cases 72 and 152). The results obtained for these two new test cases are similar to those obtained with the coarse grid.

Correlation Crosswind–Rebound Height

Results with crosswind are summarized in Fig. 11, which displays the trajectories of the primary vortices. The altitude of rebound increases with crosswind velocity. In the same manner, the length of rebound (the distance along the x axis in which the vortices are

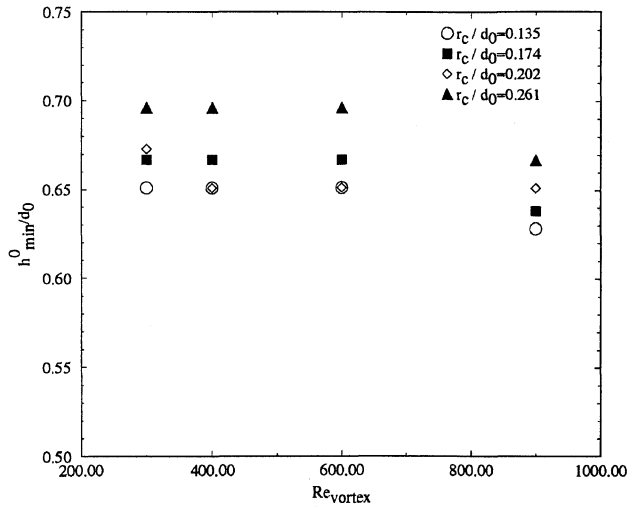

Fig. 10 Minimum altitude without crosswind.

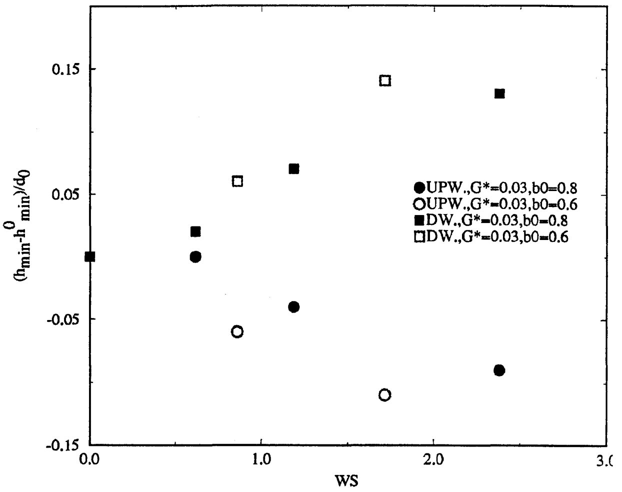

Fig. 12 Minimum altitude vs $W_S = U_0 b_0/\Gamma_0$ (UPW = upwind vortex and DW = downwind vortex).

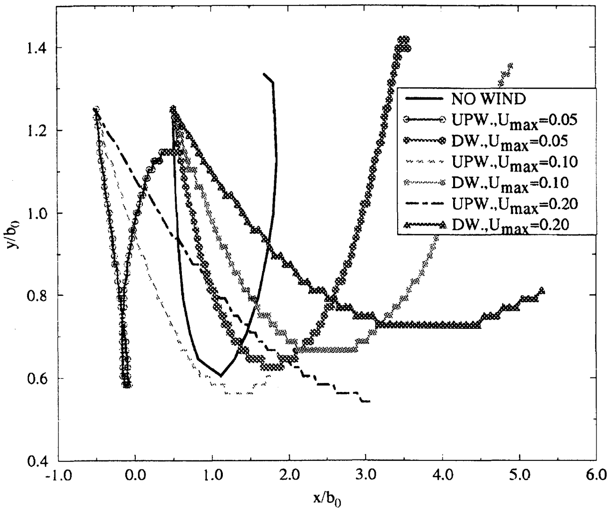

Fig. 11 Trajectories of primary vortices (UPW = upwind vortex and DW = downwind vortex).

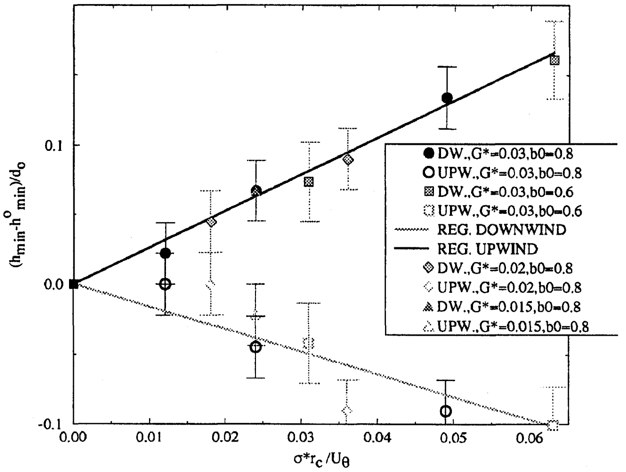

Fig. 13 Minimum altitude vs $w_s = \sigma \times r_c/u_{\theta_{max}}$ (UPW = upwind vortex and DW = downwind one).

affected by the ground) increases with crosswind. The primary vortices are advected by the crosswind, and then the area of interaction in the x direction increases as the crosswind. We have defined a dimensionless number $W_S = U_0 b_0/\Gamma_0$ (Ref. 20), where U_0 is the value of crosswind at the initial altitude, b_0 is the initial spacing between the vortices, and Γ_0 is their initial circulation. W_S is a useful parameter to describe the overall behavior of the vortices under crosswind but cannot be used to correlate the minimum altitude reached by the vortices to the crosswind characteristics; Fig. 12 displays the variation of $(h_{min} - h^0_{min})/d_0$ vs W_S, and h^0_{min} is the minimum altitude reached by the vortices without crosswind and h_{min} is the minimum altitude in the case considered.

Six different cases are plotted (1–4) plus two other cases where the initial spacing between the vortices is reduced to $b_0 = 0.6$ for two crosswind values $U^*_{max} = 0.10$ (case 5) and 0.20 (case 6). The trend varies with the initial spacing between the vortices even if the rebound mechanism is always the same.

To describe the effect of crosswind on the vortex bouncing, a better parameter is the vertical crosswind shear at an altitude of half the initial distance d_0 between the vortices

$$\sigma = \left.\frac{dU}{dy}\right|_{y=d_0/2}$$

Because the altitude of rebound depends on core radius and initial strength of the vortices,[20] an appropriate dimensionless number is

$$w_s = \frac{\sigma r_c}{u_{\theta_{max}}}$$

All previous results plus three other test cases are plotted in Fig. 13. These other cases are $g^* = 0.02$ for two values of crosswind $U^*_{max} = 0.05$ (case 7) and 0.10 (case 8) and $g^* = 0.015$ for a crosswind $U^*_{max} = 0.05$ (case 9).

The correlation between the results is good for the downwind vortices but relatively poor for the upwind ones. Error bars in Fig. 13 are due to the determination of the minimum altitude in the computation. This position can vary from ±1 grid point, giving an error of ±0.022 relative to d_0 in the case of $d_0 = 0.74$ and ±0.029 in the case of $d_0 = 0.57$.

Linear fits have been performed for the results of Fig. 13. The regression coefficient is 0.995 for the downwind vortices and −0.907 for the upwind ones. To compute the linear regression for the upwind vortex, two points are not taken into account: $g^* = 0.03$ for $U^*_{max} = 0.20$ and $g^* = 0.02$ for $U^*_{max} = 0.10$ because the downwind vortex leaves the computation domain too early.

These results lead to the following formulas.

For the downwind vortex,

$$h_{min}/d_0 = 0.65 + 2.64 w_s$$

For the upwind vortex,

$$h_{min}/d_0 = 0.65 - 1.61 w_s$$

Conclusions

Many DNS (31 cases) have been performed to study the effect of crosswind on vortex pair rebound. With or without crosswind, the vortices descend toward the ground and create a secondary vortex

The presence of crosswind induces a boundary layer with negative vorticity, which acts on the creation of secondary vortices. There is a redistribution of the vorticity induced by the primary vortices and that contained in the boundary layer. The rebound of the vortex pair is then asymmetric. The sudden eruption of wall vorticity is favored in one case (downwind), when the crosswind shear and the secondary vortex have the same sign, and counteracted in the other (upwind), where the crosswind shear and the secondary vortex have the opposite sign. In the case of high crosswind (and high shear), the upwind vortex does not rebound and follows the inviscid theory trajectory. These computations show that the experimentally observed vortex tilting in the case of crosswind can be explained by the difference in rebound height between the two vortices. As the upwind vortex descends closer to the ground than the downwind one, the influence of its image vortex is more important than its lateral velocity.

Finally, these computations allow us to define a new dimensionless parameter w_s, which gives the altitude of rebound as a function of crosswind and vortex characteristics. This parameter can be used in simple engineering models to predict rebound. This kind of study has now been extended to include three-dimensional effects and turbulence. Both effects have a great influence but the approximation of a laminar boundary layer remains valid for some typical meteorological conditions. In this case, the three-dimensional effects are important to study the instabilities of the primary–secondary vortex pair, which could explain the shortened life span of the vortices near the ground, as observed experimentally.

Acknowledgments

This work was supported by the Service Technique Navigation Aérienne under Research Grant STNA/95/110. The authors would like to thank the Commissariat à l'Energie Atomique Saclay and Centre National Universitaire Sud de Calcul for the access to their IBM SP2. The authors would like also to thank M. Baum for NTMIX developments.

References

[1]Crow, S., "Stability Theory for a Pair of Trailing Vortices," *AIAA Journal*, Vol. 8, No. 12, 1970, pp. 2172–2179.

[2]Liu, H., "Tow-Tank Simulation of Vortex Wake Dynamics," *FAA Proceedings of the Aircraft Wake Vortices Conference* (Washington, DC), edited by J. N. Hallock, 1991, pp. 32-1–32-26.

[3]Sarpkaya, T., and Daly, J., "Effect of Ambient Turbulence on Trailing Vortices," *Journal of Aircraft*, Vol. 24, June 1987, pp. 399–404.

[4]Tombach, I., "Observations of Atmospheric Effects on Vortex Wake Behavior," *Journal of Aircraft*, Vol. 10, Nov. 1973, pp. 641–647.

[5]Donaldson, C. D., and Bilanin, A., "Vortex Wakes of Conventional Aircraft," AGARDograph 204, May 1975.

[6]Greene, G., "An Approximate Model of Vortex Decay in the Atmosphere," *Journal of Aircraft*, Vol. 23, July 1986, pp. 566–573.

[7]Hill, F., "A Numerical Study of the Descent of a Vortex Pair in a Stably Stratified Atmosphere," *Journal of Fluid Mechanics*, Vol. 71, 1975, pp. 1–13.

[8]Sarpkaya, T., "Trailing Vortices in Homogeneous and Density-Stratified Media," *Journal of Fluid Mechanics*, Vol. 136, 1983, pp. 85–109.

[9]Spalart, P., "On the Motion of Laminar Wing Wakes in a Stratified Fluid," *Journal of Fluid Mechanics*, Vol. 327, 1996, pp. 139–160.

[10]Critchley, J., and Foot, P., "UK CAA Wake Vortex Database: Analysis of Incidents Reported Between 1982 and 1990," Civil Aviation Authority, CAA Paper 91, 1991.

[11]Robins, R., and Delisi, D., "Potential Hazard of Aircraft Wake Vortices in Ground Effect with Crosswind," *Journal of Aircraft*, Vol. 30, No. 2, 1993, pp. 201–206.

[12]Zheng, Z., and Ash, R., "Viscous Effects on a Vortex Wake in Ground Effect," *FAA Proceedings of the Aircraft Wake Vortices Conference* (Washington, DC), edited by J. N. Hallock, No. DOT/FAA/SD/92/1.1-1.2, 1991, pp. 31-1–31-30.

[13]Zheng, Z., Ash, R., and Greene, G., "A Study of the Influence of Cross Flow on the Behavior of Aircraft Wake Vortices Near the Ground," *Proceedings from the 18th Congress of the International Council of the Aeronautical Sciences* (Anaheim, CA), AIAA, Washington, DC, 1994, pp. 1649–1659.

[14]Luton, A., Ragab, S., and Telionis, D., "Interaction of Spanwise Vortices with a Boundary Layer," *Physics of Fluids*, Vol. 2, Nov. 1995, pp. 2757–2765.

[15]Ash, R., and Zheng, Z., "Cross Wind Effects on Turbulent Aircraft Wake Vortices Near the Ground," AIAA Paper 94-2381, June 1994.

[16]Zheng, Z., and Ash, R., "Prediction of Turbulent Wake Vortex Near the Ground," *Transitional and Turbulent Compressible Flows*, edited by L. D. Krol and T. A. Zang, ASME Fluids Engineering Conf. (Washington, DC), ASME FED Vol. 151, American Society of Mechanical Engineers, New York, 1993, pp. 195–201.

[17]Risso, F., Corjon, A., and Stoessel, A., "Direct Numerical Simulation of Trailing Vortices in Homogeneous Turbulence," AIAA Paper 96-0802, Jan. 1996.

[18]Corjon, A., Risso, F., Stoessel, A., and Poinsot, T., "3D Direct Numerical Simulations of Wake Vortices: Atmospheric Turbulence Effects and Rebound with Crosswind," *78th Fluid Dynamics Panel Symposium on the Characterization and Modification of Wakes from Lifting Vehicles in Fluids* (Trondheim, Norway), Vol. NATO-AGARD-CP-584, 1996, pp. 28-1–28-21.

[19]Doligalski, T., Smith, C., and Walker, J., "Vortex Interactions with Walls," *Annual Review of Fluid Mechanics*, Vol. 26, 1994, pp. 573–616.

[20]Corjon, A., and Poinsot, T., "Vortex Model to Define Safe Aircraft Separations Distances," *Journal of Aircraft*, Vol. 33, No. 3, 1996, pp. 547–553.

[21]Dee, F., and Nicholas, O., "Flight Measurements of Wing Tip Vortex Motion Near the Ground," Royal Aircraft Establishment, TR 68007, London, 1968.

[22]Harvey, J., and Perry, F., "Flowfield Produced by Trailing Vortices in the Vicinity of the Ground," *AIAA Journal*, Vol. 9, No. 8, 1971, pp. 1659, 1660.

[23]Barker, S., and Crow, S., "The Motion of Two-Dimensional Vortex Pairs in a Ground Effect," *Journal of Fluid Mechanics*, Vol. 82, No. 4, 1977, pp. 659–671.

[24]Saffman, P., "The Approach of a Vortex Pair to a Plane Surface in Inviscid Fluid," *Journal of Fluid Mechanics*, Vol. 92, 1979, pp. 497–503.

[25]Bilanin, A., Teske, M., and Hirsh, J., "Neutral Atmospheric Effects on the Dissipation of Aircraft Vortex Wakes," *AIAA Journal*, Vol. 16, No. 9, 1978, pp. 956–961.

[26]Orlandi, P., "Rebound of Vortex Dipole," *Physics of Fluids*, Vol. 2, No. 8, 1990, pp. 1429–1436.

[27]Baum, M., "Etude de l'Allumage et de la Structure des Flammes Turbulentes," Ph.D. Thesis, École Centrale Paris, France, 1994.

[28]Lele, S. K., "Compact Finite Difference Schemes with Spectral-Like Resolution," *Journal of Computational Physics*, Vol. 103, 1992, pp. 16–42.

[29]Poinsot, T., and Lele, S., "Boundary Conditions for Direct Simulations of Compressible Viscous Flows," *Journal of Computational Physics*, Vol. 101, July 1992, pp. 104–129.

[30]Lissaman, P., Crow, S., MacCready, P., Tombach, I., and Bate, E., "Aircraft Vortex Wake Descent and Decay Under Real Atmospheric Effects," U.S. Dept. of Transportation, FAA-RD-73-120, Cambridge, MA, Oct. 1973.

[31]Betz, A., "Verhaltern von WirbelSystemen," *ZAMM*, Vol. 12, No. 3, 1932, pp. 164–174.

[32]Lamb, H., *Hydrodynamics*, Dover, New York, 1932, p. 224.

[33]Peace, A., and Riley, N., "A Viscous Vortex Pair in Ground Effect," *Journal of Fluid Mechanics*, Vol. 129, 1983, pp. 409–426.

S. Glegg
Associate Editor